Combining automatic angle correction and 3-D tracking Doppler for the assessment of aortic stenosis severity

Stefano Fiorentini*†, Torvald Espeland*†‡, Erik Andreas Rye Berg*†‡, Svend Aakhus*†‡, Hans Torp*†, Jørgen Avdal*†

*Department of Circulation and Medical Imaging, Norwegian University of Science and Technology, Trondheim, Norway

†Centre for Innovative Ultrasound Solutions, Trondheim, Norway

‡Clinic of Cardiology, St. Olavs Hospital, Trondheim, Norway

Email: stefano.fiorentini@ntnu.no

***Abstract*—Aortic valve stenosis (AS) is a narrowing of the aortic valve opening, which causes increased load on the left ventricle. Untreated, this condition can eventually lead to heart failure and death. According to current recommendations, accurate diagnosis of AS mandates the use of multiple acoustic windows to determine the highest velocity. Furthermore, optimal positioning of both patient and transducer to reduce the beam-to-flow angle is emphasised. Being operator dependent, beam alignment is a potential source of uncertainty.**

In this work, we perform non-compounded 3-D plane wave imaging for retrospective estimation of maximum velocities in aortic jets with automatic angle correction. This is achieved by combining an hybrid 3-D speckle tracking method to estimate the jet direction, and 3-D tracking Doppler to generate angle-corrected sonograms, using the direction from speckle tracking as input.

Results from simulations of flow through an orifice show that 3-D speckle tracking can estimate the jet orientation with acceptable accuracy for signal-to-noise ratios above 10 dB. Results from 12 subjects show that sonograms recorded from a standard apical view using the proposed method yield a maximum velocity that matches CW Doppler sonograms recorded from the acoustic window with the lowest angle within a $\pm 10\%$ margin, provided that a high enough PRF could be achieved. These results motivate further validation and optimisation studies.

I. Introduction

Aortic valve stenosis (AS) is a narrowing of the aortic valve opening which increases afterload on the left ventricle. Untreated, this condition can lead to myocardial hypertrophy, fibrosis and eventually heart failure [1].

Echocardiography is the primary method for the clinical assessment of AS [2] [3]. The evaluation of AS relies on several haemodynamic parameters such as peak jet velocity, mean transvalvular pressure gradient and aortic valve area, which are based on Continuous Wave (CW) Doppler measurements and are therefore angle dependent. To align the ultrasound beam with the aortic jet, it is recommended to perform CW Doppler from several acoustic windows. Being operator dependent, beam alignment is a source of uncertainty in the assessment of AS severity.

Blood speckle tracking is a method for angle independent blood velocity measurements [4] [5], whose feasibility for quantitative flow assessment has been shown in vascular [6], cardiac [7] and pediatric applications [8]. The feasibility of blood speckle tracking for flow quantification of valvular jets has been investigated in pediatric applications using linear probes [9], but it has not been investigated in adults using phased array probes. Because of the low spatial resolution available in cardiac imaging, speckle-tracking alone is not expected to resolve the maximum velocity in valvular jets, where velocity gradients occur. This limitation would be challenging in AS severity estimation, because peak jet velocity and mean gradient are based on the maximum velocity trace.

In this paper, which is an extension of a previously presented conference proceeding [10], we propose to estimate velocity spectra of aortic jets with automatic angle correction. This is achieved using non-compounded 3-D plane-wave imaging and a two-step method. First, a hybrid 3-D speckle tracking method [11] is used to estimate the valvular jet direction. The direction is then used to estimate angle-corrected velocity spectra using 3-D tracking Doppler [12], a wide-band spectral estimator. A feasibility study of the method is conducted on simulated data and on a small group of patients in a wide range of AS severities. We decided to limit the investigation to peak jet velocity, since it is regarded as the strongest predictor of clinical outcome [2], Moreover, the peak jet velocity is also used to diagnose aortic sclerosis and very severe aortic stenosis [3]. The method may reduce the inter- and intra-operator variability in the clinical assessment of AS, by removing the need to perform CW Doppler from multiple acoustic windows.

The method and the main details of 3-D tracking Doppler and 3-D speckle tracking are presented in Section II. A feasibility study based on *in silico* and *in vivo* datasets, is described in Section III. The results are shown in Section IV and discussed in Section V.

II. Methods

The framework consists of three steps: clutter filtering, beam-to-flow angle estimation and spectral estimation.

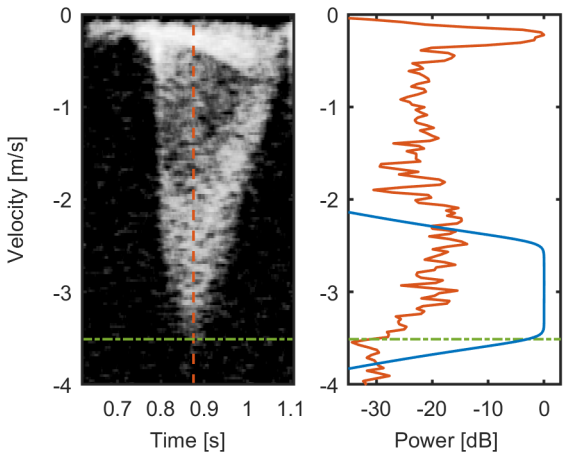

Fig. 1. The left panel shows an example of an *in vivo* PW Doppler sonogram. The maximum velocity (green dotted line) is identified by visual inspection. The power spectrum (solid orange) shown in the right panel is extracted from the time instant highlighted in the left panel. The frequency response of the Butterworth filter (blue solid line) is also shown.

A. Clutter filter

In order to mitigate speckle decorrelation and improve tracking of the highest velocities, a complex band-pass filter was applied before speckle tracking. The use of complex-valued filters was motivated by the need to filter those datasets in which the maximum Doppler shift lay between the Nyquist velocity and twice the Nyquist velocity. The maximum Doppler shift was manually identified in each dataset after visual inspection of the PW sonogram. The Butterworth filter was designed with a high -3dB cutoff equal to the maximum Doppler shift and a bandwidth equal to 30% of the maximum Doppler shift. An example of the filter design process is shown in Figure 1.

B. Jet direction estimation

The aortic jet direction was estimated using the hybrid blood speckle tracking approach described by Wigen et al. [11]. In this method a 3-D blood velocity vector field was obtained by combining phase and envelope information. Blood speckle tracking was performed in the region with the highest power of the autocorrelation function.

The axial velocity component was first estimated from the autocorrelation function. The autocorrelation function was averaged over a 4x4x4 mm spatial region and over a packet of 10ms x PRF samples before extracting the phase. The azimuth and elevation velocity components were estimated in a second step by performing block matching on envelope data. Block matching was performed using a 3-D search kernel that was displaced along the axial direction according to the component estimated in the first step. The azimuth and elevation components were estimated by maximising the normalised cross-correlation function

$$\Phi(\alpha,\beta) = \frac{\sum_{x,y}(I_{(x-\alpha,y-\beta)} - \bar{I})(K_{(x,y)} - \bar{K})}{\sqrt{\sum_{x}(I_{(x-\alpha,y-\beta)} - \bar{I})^2 \sum_{y}(K_{(x,y)} - \bar{K})^2}} \quad (1)$$

where I is the search kernel evaluated at lag 1, K is the reference kernel, $\bar{I}$ and $\bar{K}$ denote the average in the reference and search kernels respectively and (α,β) is the displacement of the search kernel from the reference kernel along azimuth and elevation. The kernel size was set according to the estimated spatial resolution. The lateral kernel size was set to $1.2\lambda f_{\#}$, where $f_{\#}$ is the f-number. The radial kernel size was set to $0.5N_c\lambda$, where N_c is the number of pulse cycles. Therefore, different kernel sizes were employed depending on the imaging depth, which could vary significantly between subjects. Speckle tracking was carried out over a few consecutive packets of 10 ms at peak systolic velocity. Finally, the forward-backward tracking approach described in [8] was adopted to enhance the tracking accuracy in datasets with low signal-to-noise and signal-to-clutter ratios.

The jet direction was estimated from the vector flow data in a two-step process. First, the histograms for the three velocity components were extracted from the vector velocity field estimated in the region of interest, as shown in Figure 2. Finally, the three components of the jet direction were computed as the mean, the median or the mode of the velocity histograms.

C. Spectral estimation

Velocity spectra were estimated using 3-D tracking Doppler, a wide-band spectral estimator that has been presented previously [12]. In 3-D tracking Doppler a full velocity spectrum is estimated from a complex-envelope 3-D + time dataset $s_{IQ}(\vec{x},k)$ where $\vec{x}$ is a vector that defines the spatial coordinates and $k \in [1,K]$ is the frame number. Spectral estimation is accomplished in two steps.

For every velocity v of interest, a packet with $2N+1$ samples is interpolated along a straight line for every frame. The interpolated signal is a function of the position along the tracking direction and slow-time and can be interpreted as a pseudo M-Mode matrix. A new pseudo M-Mode matrix is generated for every velocity.

The spectral power $\hat{P}(v,k)$ is estimated by squaring the sum of samples in each packet, which is equivalent to squaring the sum of elements in the pseudo M-Mode matrix along the main diagonals

$$\hat{P}(v,k) = \left| \sum_{n=-N}^{N} w(n)\hat{s}(\vec{x}_0 + nT\vec{v}, k+n) \right|^2 \quad (2)$$

where n is the sample index in a packet, $T = 1/PRF$ is the pulse repetition period, $w(n)$ is a window function to reduce side lobes in the spectrum, $\vec{x}_0$ denotes the spatial coordinates of the sample with index $n=0$, $\vec{v}$ is a vector with magnitude equal to the velocity being estimated and direction equal to the prescribed tracking direction. The phase correction term

$$\hat{s}(\vec{x},k) = s_{IQ}(\vec{x},k)e^{i2\pi f_d \vec{x}\cdot\vec{a}} \quad (3)$$

is applied to ensure that signal from different depths are summed coherently, where f_d is the demodulation frequency and $\bar{a}$ is a unit vector that defines the propagation direction of the transmit beam.

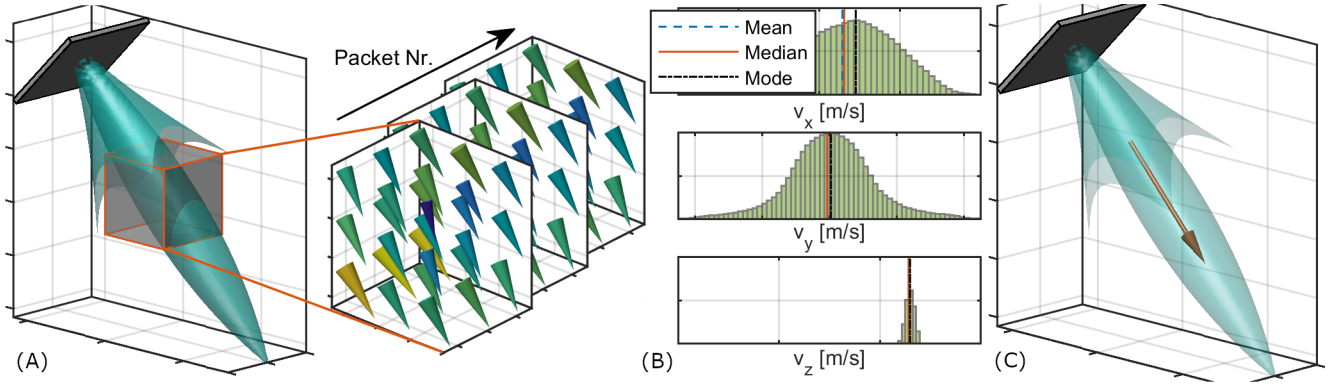

Fig. 2. Depiction of the jet direction estimation process. In panel (A) an ideal jet flow is depicted. The vector velocity field is estimated in a small region of interest placed at the jet. In panel (B) the vector velocity estimates from a few consecutive packets are used to estimate a histogram for each velocity component. The components of the aortic jet direction, shown in panel (C), are extracted from the mean, median or mode of each histogram.

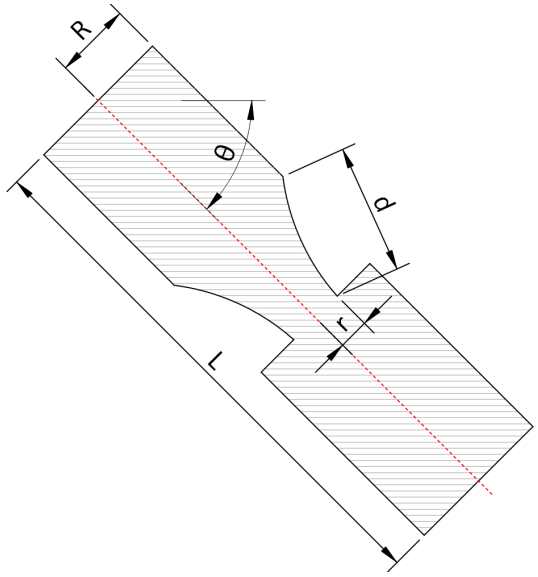

Fig. 3. Template for the aortic stenosis phantoms used in the computational fluid dynamics simulations. The numeric values used for the parameters are shown in Table I .

TABLE I
IN SILICO PHANTOM PARAMETERS

Parameter	Symbol	Value
LVOT radius	R	1 [cm]
Aortic Valve radius	r	0.66 - 0.56 - 0.45 [cm]
Aortic Valve Area	Σ	1.36 - 0.98 - 0.63 [cm^2]
Phantom length	L	7 [cm]
Leaflet length	d	~1.5 [cm]
LVOT velocity	v	1 [m/s]
Signal to Noise Ratio	SNR	6 - 10 - 20 [dB]
Beam-to-flow angle	θ	0 - 20 - 40 - 60 [°]

III. VALIDATION

A. In silico validation

The performance of the proposed method was measured using synthetic data. Stationary flow through an ideal stenotic aortic valve was simulated using the Computational Fluid Dynamics (CFD) software ANSYS Fluent (R19.0, ANSYS, Inc.). The software computed the velocity and pressure fields over a discrete domain by solving the Navier-Stokes equations. Turbulence was taken into consideration using the simplified $k-\varepsilon$ equation. To reduce computational load, axial symmetry was assumed for the geometry. Three different grades of stenosis severity where simulated by setting the aortic valve area to 1.36, 0.98 and 0.63 cm^2 respectively. Blood was modelled as an incompressible, newtonian fluid with density and viscosity equal to $\rho = 1060$ [kg/m^3] and $\nu = 3.5 \times 10^{-3}$ [kg/m s] respectively. A flat velocity profile of 1 m/s was set at the inlet, which is consistent with LVOT velocity measurements in patients during peak systole. A template of the phantom geometry is shown in Figure 3, whereas the parameters used in the simulations are shown in Table I.

The maximum velocity magnitudes for the three simulated phantoms were 2.4, 3.2 and 5.1 m/s, respectively. The velocity field for phantom P3 is depicted in Figure 4.

The velocity field was used to propagate point scatterers in a Field II simulation [13] [14] on MATLAB (2017b, The Mathworks, Natick, MA, USA), using the approach described by Swillens [15]. The phantoms were displaced to position the jet at the center of the transducer aperture and at a depth of 10 cm, resembling the typical depth of the aortic valve from an apical five-chamber view. Several ultrasound simulations were generated from each CFD phantom by rotating the phantom in the azimuth plane to achieve $\theta = [0, 20, 40, 60]°$ beam-to-flow angles. The phantoms were filled with randomly positioned point scatterers to achieve a density of 10 scatterers per resolution cell. This density value was chosen to ensure normally distributed RF signals and fully developed speckle, while keeping the computational load as low as possible. Flow data was recorded using a non-compounded plane wave acquisition scheme. RF channel data sampling rate was set to 100 MHz to avoid aliasing. The acquisition parameters are given in Table II. GE 4V-D transducer geometry (20.6 mm azimuth aperture, 16.5 mm elevation aperture, 0.343 mm pitch, 60 azimuth elements, 48 elevation elements) and impulse response were used.

Synthetic RF channel data were processed using the Ultrasound Toolbox (USTB) [16]. Data were first band-pass filtered, complex demodulated and decimated. The demodulation fre-

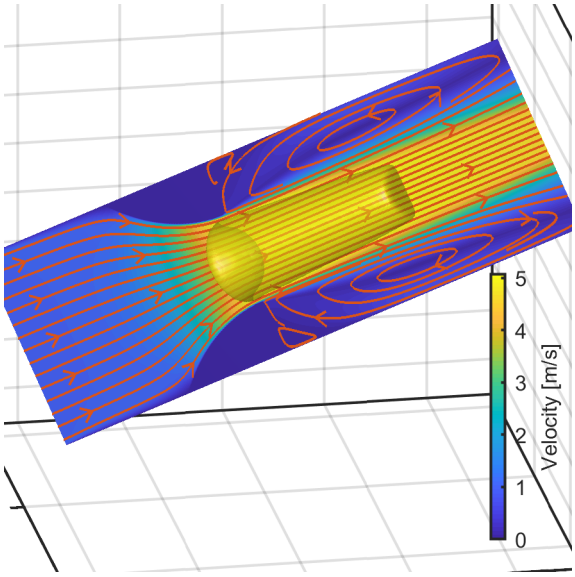

Fig. 4. Velocity field for phantom P3. Since axial symmetry was prescribed in the simulations, only a longitudinal cut-plane is shown. The iso-surface delimits the volume where the velocity magnitude was ≥ 5 [m/s]. The length of the iso-surface is 2 cm.

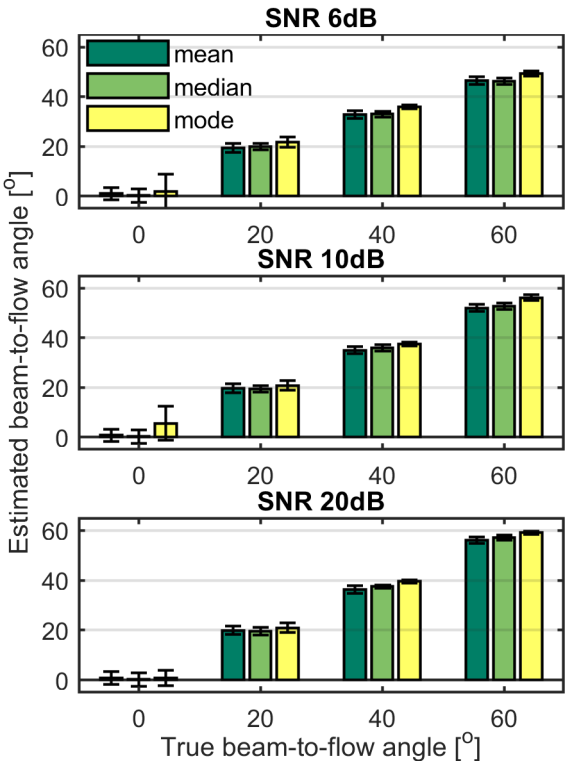

Fig. 5. Bar plots of the estimated beam-to-flow angles vs true beam-to-flow angle for mean, median and mode estimators. The error bars depict the standard deviation over 5 measurements

quency was set as the centre frequency of the convolution between the transducer's impulse response and the excitation. Channel data were beamformed with a conventional delay-and-sum algorithm without apodization. White Gaussian noise was added to beamformed data to achieve 6, 10 or 20 dB signal-to-noise ratios (SNR). Five realizations, each 10 ms long, were simulated for each combination of SNR, beam-to-flow angle and stenosis degree.

The method described in Section II was applied on each realization to estimate the jet flow direction and the 3-D tracking Doppler sonogram. Bias and standard deviation of the method over the realizations were used as performance metrics.

B. In vivo validation

The proposed method was tested on a group of 12 subjects, 2 controls and 10 patients, covering a wide range of AS severity. The recordings were performed as part of the clincal study "Ultrasonic Markers for Myocardial Fibrosis and Prognosis" (clinicaltrials.gov - NCT03422770). The trial was approved by the Norwegian Regional Committee for Medical and Health Research Ethics, and all the subjects provided written informed consent. Recordings were performed by an expert echocardiographer using a GE E95 ultrasound scanner equipped with a GE 4V-D matrix transducer (GE Vingmed Ultrasound, Horten, Norway). The scanner was locally modified to enable non-compounded plane wave acquisitions when operating in PW Doppler mode. Navigation was performed using a focused, 2-D B-mode imaging sequence and the transducer was positioned to achieve a standard apical five-chamber view. The echocardiographer located the aortic valve region and froze the B-Mode sequence to enable PW Doppler imaging using plane waves. The real-time PW Doppler spectrum was used for quality assurance only, while 1.5 s of channel data were stored for offline processing. The acquisition parameters are given in Table II. High PRF mode was enabled to avoid aliasing of the highest velocities at the cost of depth ambiguity. In several cases, strong echoes arising from tissue regions in the nearfield could saturate the front-end and corrupt the blood signal. Therefore, the PRF was adjusted in every recording to avoid this instance. Typical *in vivo* PRF values were in the range 10-18 kHz. Channel data were beamformed and post-processed offline using USTB and MATLAB. Angle-corrected PW Doppler and 3-D tracking Doppler sonograms were generated using the framework described in Section II. PW spectra were averaged in space to reduce variance and both PW and 3-D tracking Doppler spectra were averaged in time using a 20 ms moving average filter.

The velocity spectra were stored as anonymous DICOM files and analysed by two expert clinicians using ECHOPAC (202.53, GE Vingmed Ultrasound, Horten, Norway), who measured the peak systolic velocity. The peak systolic velocity was also measured in standard CW sonograms, which were recorded during standard clinical examinations using a GE M5s-D phased array probe or a GE P2D dual element probe. Standard CW Doppler recordings were performed immediately before or after the 3-D Doppler recordings to reduce the effects of variability in physiological parameters that could affect aortic flow (i.e. heart rate and blood pressure). The clinicians were blinded when performing the analysis.

TABLE II
IN SILICO AND IN VIVO SETUP PARAMETERS

ACQUISITION			POST PROCESSING		
Parameter	Symbol	Value	Parameter	Symbol	Value
Transmit frequency	f_0	2 [MHz]	Bandpass filter		Butterworth 8
Pulse Repetition Frequency	PRF	10-18 [kHz]	Filter bandwidth	Δf	$0.3 \times f_{max}$
Pulse cycles at f_0	N_c	3.5	Window size	$2N+1$	10 [ms] $\times$ PRF
IQ sampling frequency	f_s	4.5 [MHz]	Window type		Hamming
Demodulation frequency	f_d	1.9 [MHz]	Tracking length	l	1 [cm]

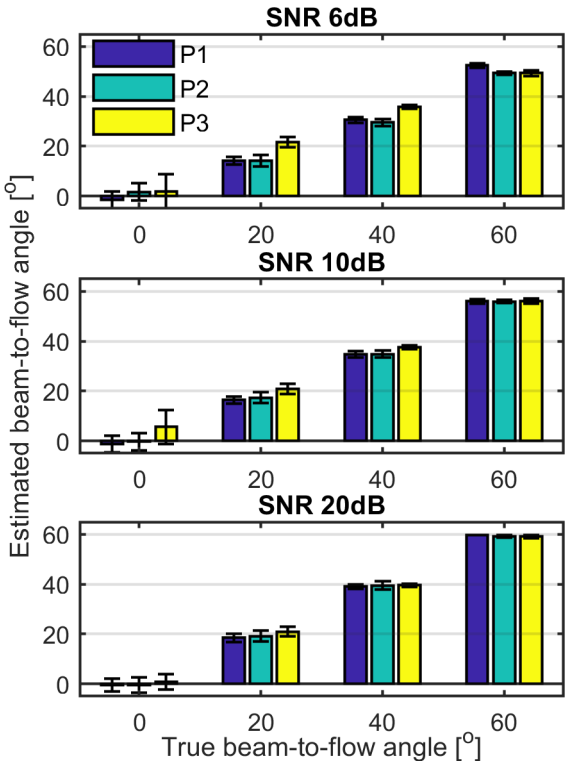

Fig. 6. Bar plot depicting the estimated beam-to-flow angles vs true beam-to-flow angle for the mode estimator. Results are shown for three degrees of aortic stenosis at [0, 20, 40, 60]° beam-to-flow angles and [6, 10, 20] dB SNR. The maximum velocity magnitudes are 2.4, 3.2 and 5.1 m/s for phantoms P1, P2 and P3 respectively.

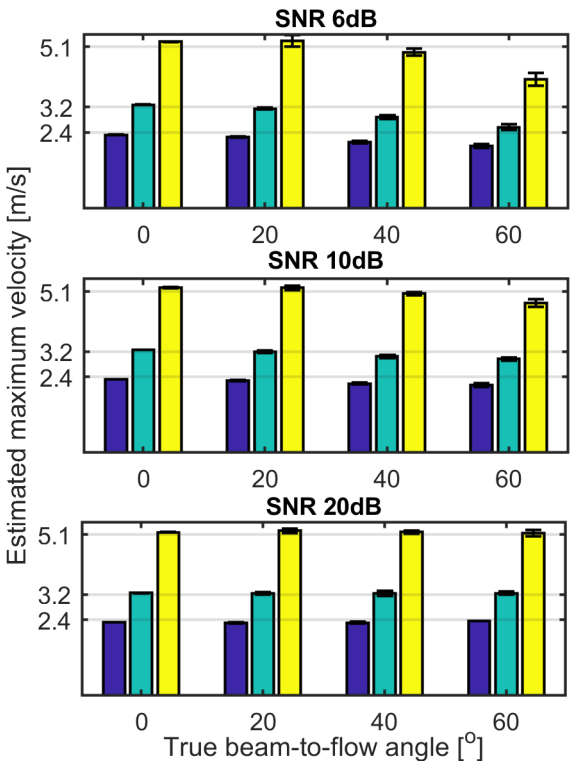

Fig. 7. Bar plot depicting the estimated -6dB maximum velocity for three degrees of aortic stenosis severity. The maximum velocity magnitudes are 2.4, 3.2 and 5.1 m/s for phantoms P1, P2 and P3, respectively. Results are shown for [0, 20, 40, 60]° beam-to-flow angles and [6, 10, 20] dB SNR. 3-D tracking Doppler was estimated along the same direction used to generate the results in Figure 6.

IV. RESULTS

A. Simulation study

In Figure 5 the estimated beam-to-flow angle for phantom P3 (AVA 0.63 cm^2, maximum velocity 5.1 m/s) is shown as a function of the true beam-to-flow angle. The angles estimated using the mean, median and mode are compared at 6, 10 and 20 dB SNR. Results show that the mode estimator delivered between $2°$ and $4°$ reduced bias compared to the mean and median estimators. Results also show that the method underestimated the angle for SNR below 20dB, regardless of the estimator used. This effect is evident at higher beam-to-flow angles. For example, the mode estimator shows a $5°$ and $11°$ bias at $40°$ and $60°$ beam-to-flow angles and 6 dB SNR, while it shows a $3°$ and $4°$ bias at $40°$ and $60°$ beam-to-flow angles and 10 dB SNR.

In Figure 6 the estimated beam-to-flow angle using the mode estimator is shown as a function of the true beam-to-flow angle. Angle estimates are shown for three simulated grades of aortic stenosis, denoted as P1, P2 and P3 at 6, 10, and 20 dB SNR. The grade of aortic stenosis did not have a significant impact on the bias of the mode estimator. As mentioned previously, the method underestimated the angle for signal-to-noise ratios below 20 dB. The bias at $60°$ beam-to-flow angle dropped from $11°$ at 6 dB SNR to $4°$ at 10 dB SNR.

In Figure 7 the maximum velocity from 3-D tracking Doppler is shown as a function of the true beam-to-flow angle. The maximum velocity was estimated as the velocity whose power spectrum is equal to -6 dB below the maximum power, along the descending slope of the spectrum. 3-D tracking Doppler was estimated along the directions that provided the

TABLE III
IN VIVO RESULTS

Subject Nr.	PW Doppler			3-D Tracking Doppler			CW Doppler		
	Observer 1	Observer 2	Mean	Observer 1	Observer 2	Mean	Observer 1	Observer 2	Mean
1	1.10	0.95	1.03	1.00	1.00	1.00	1.20	1.15	1.18
2	5.70	6.07	5.89	5.70	5.77	5.74	5.30	5.34	5.32
3		X		3.70	3.62	3.66	3.30	3.52	3.41
4	4.50	4.30	4.40	3.60	3.59	3.60	4.00	3.97	3.99
5	2.60	2.39	2.50	2.60	2.59	2.60	2.90	3.07	2.99
6	1.90	1.22	1.55	2.00	1.30	1.65	2.90	2.11	2.51
7		X		3.60	3.45	3.53	3.3	3.60	3.45

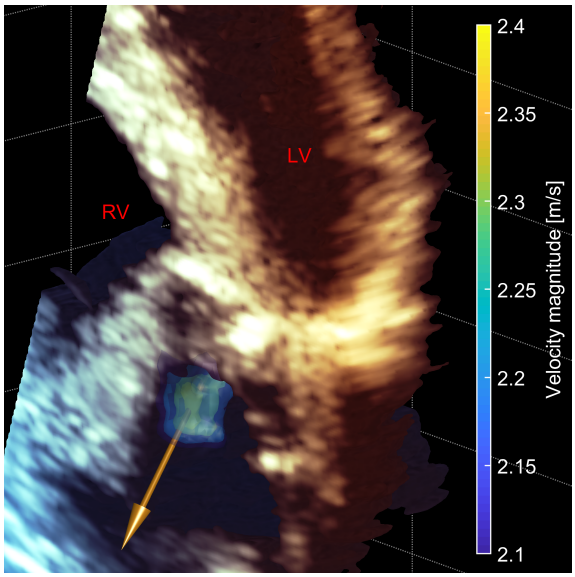

Fig. 8. *In vivo* 3-D duplex rendering of subject 7 during peak systole. Left Ventricle (LV) and Righ Ventricle (RV) cavities are marked. The arrow indicates the estimated aortic jet direction. The beam-to-flow angle was 28°.

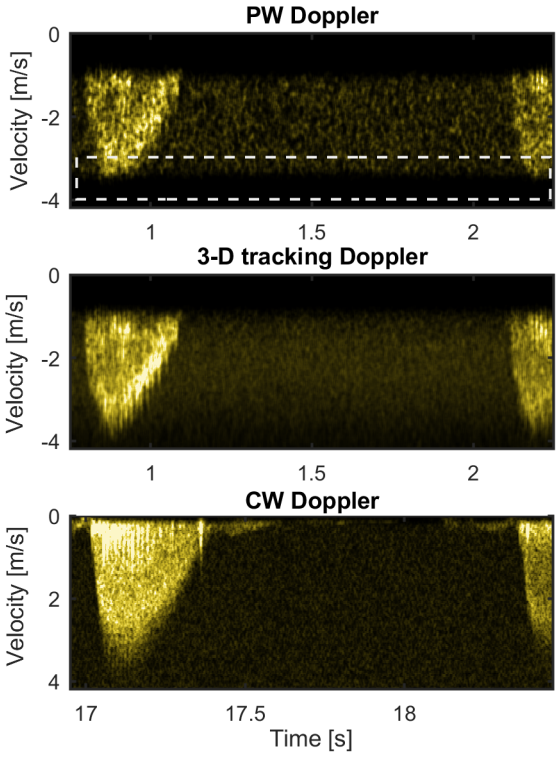

Fig. 9. *In vivo* example of velocity spectra from subject 7, whose results are summarised in Table III. The estimated beam-to-flow angle was 28°. A CW Doppler spectrum from a more lateral apical view is shown for reference. The white box highlights the region in the PW Doppler spectrum where the signal is attenuated by the clutter filter.

results in Figure 6, and the results are depicted using the same colour coding. Results show that the underestimation of the beam-to-flow angle caused an underestimation of the maximum velocity from 3-D tracking Doppler. The underestimation was significant at 60° beam-to-flow angle and 6 dB SNR, where an 11° bias caused an underestimation of the maximum velocity by 0.45, 0.65, and 1.05 m/s for phantoms P1, P2 and P3 respectively. On the other hand, the underestimation was less critical at 60° beam-to-flow angle and 10 dB SNR, where a 4° bias caused an underestimation of the maximum velocity by 0.25, 0.2, and 0.35 m/s for phantoms P1, P2 and P3 respectively

B. *In vivo study*

In Table III the peak systolic velocities for CW Doppler, PW Doppler and 3-D tracking Doppler are shown for 7 out of the 12 investigated subjects. Four subjects were discarded because the achieved PRF was too low and the peak systolic velocity was above twice the Nyquist limit. One subject was discarded because of arrhythmia. 3-D Doppler data were recorded from a standard apical five-chamber view and were processed using the framework described in Section II, while CW Doppler recordings were performed from multiple acoustic windows (apical, suprasternal, right parasternal and subcostal) during a standard clinical investigation. Only the CW recording that yielded the highest maximum velocity was taken into consideration. The measurements marked with a cross in Table III were discarded by the clinicians because the clutter filter suppressed the highest portion of the spectrum.

In Figure 8 a 3-D duplex rendering for subject 7 during peak systole is shown. The arrow indicates the aortic jet direction estimated using speckle tracking.

In Figure 9 PW Doppler, 3-D tracking Doppler and CW Doppler sonograms for subject 7 are compared. The estimated beam-to-flow angle was 28°. The CW Doppler spectrum that yielded the highest peak systolic velocity was recorded from a more lateral apical view. In this example it was necessary to

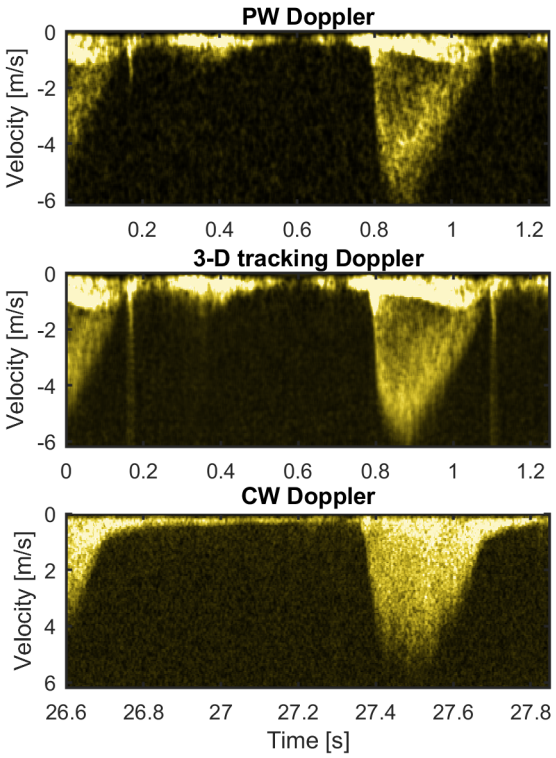

Fig. 10. *In vivo* example of velocity spectra from subject 2, whose results are summarised in Table III. The estimated beam-to-flow angle was $57°$. A CW Doppler spectrum from a right parasternal view is shown for reference.

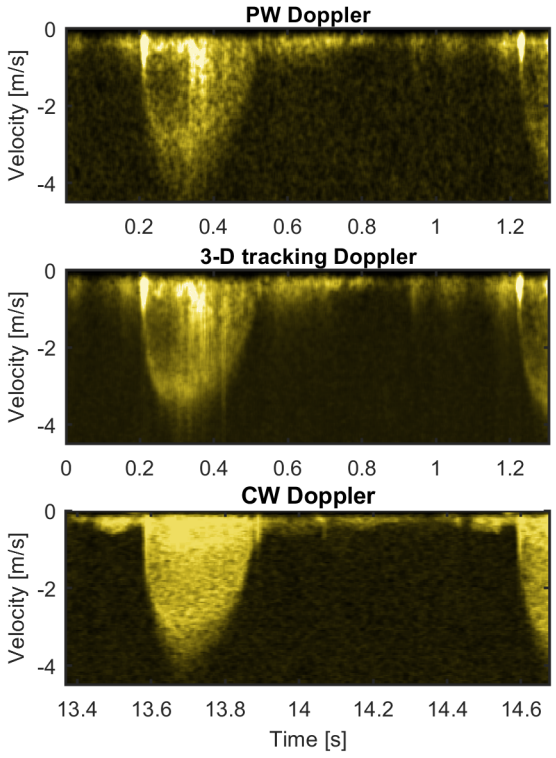

Fig. 11. *In vivo* example of velocity spectra from subject 4, whose results are summarised in Table III. The estimated beam-to-flow angle was $38°$. A CW Doppler spectrum from an apical short-axis view is shown for reference.

set the cut-off velocity to 1 m/s to suppress sidelobes arising from fast moving clutter. The combination of high cut-off and low PRF caused the highest portion of the PW spectrum to be attenuated by the clutter filter. In 3-D tracking Doppler the signal level is retained, although the noise floor is suppressed. The measured peak systolic velocities were 3.5 and 3.4 m/s for 3-D tracking Doppler and CW Doppler respectively.

In Figure 10 PW Doppler, 3-D tracking Doppler and CW Doppler sonograms for subject 2 are compared. The estimated beam-to-flow angle was $57°$. The CW Doppler sonogram that yielded the highest peak systolic velocity was recorded from a right parasternal view. The measured peak systolic velocities were 5.8, 5.7 and 5.3 m/s for PW Doppler, 3-D tracking Doppler and CW Doppler respectively.

In Figure 11 PW Doppler, 3-D tracking Doppler and CW Doppler sonograms for subject 4 are compared. The estimated beam-to-flow angle was $35°$. The CW Doppler sonogram that yielded the highest peak systolic velocity was recorded from an apical view. The measured peak systolic velocities were 4.4, 3.6 and 3.9 m/s for PW Doppler, 3-D tracking Doppler and CW Doppler respectively.

V. Discussion

In this paper we have presented a method that combines blood speckle tracking and 3-D tracking Doppler to estimate velocity spectra with automatic angle correction. This feature may reduce the inter and intra operator variability of measurements in patients with AS related to manual beam alignment.

Results from Figure 5 show that the proposed method tends to underestimate the beam-to-flow angle for SNR values below 10dB. These results motivate further work into optimising both the post-processing chain and the acquisition scheme. Results also show that the mode estimator provides slightly reduced bias compared to the mean and the median, and motivate its use in the method.

Results from Figure 6 show that the performance of the mode estimator depends only to a limited extend on the degree of the aortic stenosis and that the amount of underestimation increases with the beam-to-flow angle. This implies that the most critical cases are the ones that combine low signal-to-noise ratio and high beam-to-flow angle.

Results from Figure 7 show that underestimating the beam-to-flow angle causes an underestimation of the maximum velocity. Underestimation becomes evident at 6 dB SNR and for angles above $40°$, but clinical experience indicates that the beam-to-flow angle is often below this value. Moreover, the maximum velocity is estimated accurately up to $60°$ beam-to-flow angle for signal-to-noise ratios above 10 dB. On the other hand, sub-valvular membranes and non-tricuspid valves can cause eccentric aortic jets. Therefore, cases with higher beam-to-flow angles should also be expected.

Results from Table III show that the method can deliver velocity spectra with peak systolic velocities within $\pm 10\%$ of CW Doppler measurements, which were used as reference. Underestimated velocities in subjects 4, 5 and 6 may be caused by an underestimation of the beam-to-flow angle as demonstrated in the simulation study. Moreover, the results shown

in Figure 11 highlight that another cause of underestimation could be the lower dynamic range available in 3-D tracking Doppler compared to CW. This makes it harder to differentiate between the highest velocities in the spectrum and the noise floor, motivating further work to improve acquisition and post-processing. Moreover, although CW Doppler is currently regarded as the gold standard for AS assessment, it is a surrogate of the ground truth because it depends on the ability of the examiner to align the ultrasound beam with the stenotic jet. An ongoing clinical study will compare the proposed method against CW Doppler on a larger number of subjects.

The method estimates the aortic jet direction from the mode of the velocity histogram of each velocity component after speckle tracking. It is expected to provide reliable results as long as the aortic velocity field is stationary within the spatial and temporal regions of interest. Velocity gradients that occur in jets not only have a negative impact on speckle coherency, but also change the underlying velocity distribution and increase the broadening of histograms. Therefore, the choice of spatial and temporal extent of the region of interest was a trade-off between having enough samples to generate the velocity histogram and avoiding velocity gradients.

3-D Tracking Doppler is a wide-band spectral estimator that can reduce transit time broadening by tracking the blood scatterers along a straight line [12]. 3-D tracking Doppler is based on the assumption that the phase of the blood signal is preserved along the tracking direction, and this condition is not always fulfilled in jets, where velocity gradients occur. While velocity gradients were not an issue in Figure 11 where 3-D tracking Doppler shows less spectral broadening compared to PW Doppler, they were the cause of degraded performance in Figure 10 in which PW Doppler and 3-D tracking Doppler spectra show comparable broadening. However, results also show that 3-D tracking Doppler delivered spectra with reduced variance compared to PW Doppler. A more uniform appearance may be beneficial when tracing the maximum velocity envelope, which is necessary when estimating velocity integral and mean gradient. Another advantage of 3-D tracking Doppler over PW Doppler is shown in Figure 9. In this case the clutter filter suppressed the highest blood velocities in the PW Doppler spectrum, making it impossible to evaluate the peak systolic velocity. 3-D tracking Doppler is less affected by this issue because the method is also sensitive to phase correlation along the tracking direction [17].

The synthetic phantoms were designed to mimic jet flow through a stenotic aortic valve and managed to reproduce maximum velocity magnitudes within physiological values. On the other hand, prescribing axial symmetry to reduce the computational load may lead to unrealistic results. In fact, high beam-to-flow angles were achieved in our simulations by rotating the phantom, whereas eccentric aortic jets are caused by asymmetric valve structures (e.g. bicuspid aortic valves, asymmetric calcification) or sub-valvular membranes. As previously mentioned, more complex flow configurations may impact the performance of the method. Future validation studies could involve 3-D CFD simulations based on realistic valve geometries from CT scans. Stationary flow was also assumed. Although transient simulations with a realistic LVOT velocity trend would be preferable, the stationarity assumption should hold over the duration of our simulations (10 ms). Future validation studies could also involve time-dependent simulations.

Challenges for clinical acceptance

The proposed method exhibits several critical points that must be addressed before it can be considered for clinical use. The first challenge is achieving sufficient PRF to avoid aliasing of peak systolic velocities. In our feasibility study it was not possible in 4 out of 12 patients because the signal appeared to be corrupted when the PRF was brought above the 12-15 kHz range. The problem could be caused by strong echoes arising from isolated reflectors in the near-field, which are picked by the transducer when operating in high-PRF mode. These strong echoes could cause saturation of the either the sub-aperture processors or the front-end. A possible solution could be to increase the pulse length while keeping the mean pulse power constant. The SNR of Doppler estimators would not be affected by this change, while the risk of saturation would be reduced. This solution would come at the expense of reduced axial resolution, which could impact both speckle tracking and 3-D tracking Doppler in a negative way. Another option could be to reduce the transmit power, but this would come at the cost of lower SNR.

The second challenge is coping with sensitivity of the method to noise. Simulations have shown that the accuracy of angle estimation depends on SNR. In difficult to image patients, the noise level may be too high for accurate angle estimation while being good enough for CW Doppler. The robustness of the method to noise will be investigated in a larger proof-of-concept clinical study, and further work will aim at improving the acquisition setup. Moreover, advancements in transducer technology may deliver 3-D ultrasound probes with increased dynamic range and SNR, which should help coping with the two aforementioned challenges.

The third challenge is reducing the amount of user intervention needed. In fact, both the sample volume and the wall filter cut-off are set manually. While the sample volume could be placed interactively by the clinician, as done for PW Doppler, the wall filter should be designed without user intervention. One solution could be to have automatic detection of the Doppler envelope and automatically design the wall filter depending on the peak systolic velocity. Further work will focus on automatic filter design and on the impact of different filtering strategies on the method.

A comprehensive assessment of AS is based on several clinical markers, such as mean transvalvular pressure gradient, velocity time integral (VTI) and aortic valve area (AVA). However, the feasibility analysis in this work was limited to a single parameter, peak jet velocity. The results from peak jet velocity are expected to translate to the other clinical markers, because the spectral envelope would be scaled by the same angle correction factor. An ongoing clinical study will analyse the performance of the proposed method with respect to all of the relevant clinical markers. Moreover, while the proposed method could be applied to estimate LVOT velocities, this was not done in this work.

VI. CONCLUSION

In this work we have proposed a method to estimate blood velocity spectra with automatic angle correction. The method may reduce the variability in the clinical assessment of AS by removing the need to perform CW Doppler from several acoustic windows. Results from simulations show that the method estimates beam-to-flow angles up to $60°$ with good accuracy for signal-to-noise ratios above 10 dB. *In vivo* feasibility of the method was also shown in a group of 12 subjects, and we are currently starting a larger clinical proof-of-concept study

REFERENCES

[1] S. Hein, E. Arnon, S. Kostin, *et al.*, "Progression from compensated hypertrophy to failure in the pressure-overloaded human heart: Structural deterioration and compensatory mechanisms", *Circulation*, vol. 107, no. 7, pp. 984–91, 2003.

[2] H. Baumgartner, J. Hung, J. Bermejo, *et al.*, "Recommendations on the Echocardiographic Assessment of Aortic Valve Stenosis: A focused update from the European Association of Cardiovascular Imaging and the American Society of Echocardiography", *J Am Soc Echocardiogr*, vol. 30, no. 4, pp. 372–392, 2017.

[3] H. Baumgartner, V. Falk, J. J. Bax, *et al.*, "2017 esc/eacts guidelines for the management of valvular heart disease", *Rev Esp Cardiol (Engl Ed)*, vol. 71, no. 2, p. 110, 2018.

[4] G. E. Trahey, S. M. Hubbard, and O. T. von Ramm, "Angle independent ultrasonic blood flow detection by frame-to-frame correlation of B-mode images", *Ultrasonics*, vol. 26, no. 5, pp. 271–6, 1988.

[5] L. N. Bohs, B. J. Geiman, M. E. Anderson, S. C. Gebhart, and G. E. Trahey, "Speckle tracking for multi-dimensional flow estimation", *Ultrasonics*, vol. 38, no. 1-8, pp. 369–75, 2000.

[6] A. Swillens, P. Segers, H. Torp, and L. Lovstakken, "Two-dimensional blood velocity estimation with ultrasound: Speckle tracking versus crossed-beam vector doppler based on flow simulations in a carotid bifurcation model", *IEEE Trans Ultrason Ferroelectr Freq Control*, vol. 57, no. 2, pp. 327–39, 2010.

[7] T. Hiroki, H. Hideyuki, and K. Hiroshi, "Echo speckle imaging of blood particles with high-frame-rate echocardiography", *Japanese Journal of Applied Physics*, vol. 53, no. 7S, 07KF08, 2014.

[8] S. Fadnes, M. S. Wigen, S. A. Nyrnes, and L. Lovstakken, "In vivo intracardiac vector flow imaging using phased array transducers for pediatric cardiology", *IEEE Trans Ultrason Ferroelectr Freq Control*, vol. 64, no. 9, pp. 1318–1326, 2017.

[9] J. Van Cauwenberge, L. Lovstakken, S. Fadnes, *et al.*, "Assessing the performance of ultrafast vector flow imaging in the neonatal heart via multiphysics modeling and in vitro experiments", *IEEE Trans Ultrason Ferroelectr Freq Control*, vol. 63, no. 11, pp. 1772–1785, 2016.

[10] S. Fiorentini, T. Espeland, E. A. Rye Berg, S. Aakhus, H. Torp, and J. Avdal, "Combining automatic angle correction and 3-D tracking Doppler for aortic stenosis severity assessment", in *IEEE Ultrasonics Symposium*, IEEE, pp. 1–4.

[11] M. S. Wigen, S. Fadnes, A. Rodriguez-Molares, *et al.*, "4D intracardiac Ultrasound vector flow imaging -feasibility and comparison to phase-contrast MRI", *IEEE Trans Med Imaging*, 2018.

[12] S. Fiorentini, L. M. Saxhaug, T. G. Bjastad, E. Holte, H. Torp, and J. Avdal, "Maximum velocity estimation in coronary arteries using 3-D tracking doppler", *IEEE Trans Ultrason Ferroelectr Freq Control*, vol. 65, no. 7, pp. 1102–1110, 2018.

[13] J. A. Jensen, "Field: A program for simulating Ultrasound Systems", *Medical & Biological Engineering & Computing*, vol. 34, pp. 351–353, 1996.

[14] J. A. Jensen and N. B. Svendsen, "Calculation of pressure fields from arbitrarily shaped, apodized, and excited Ultrasound transducers", *IEEE Trans Ultrason Ferroelectr Freq Control*, vol. 39, no. 2, pp. 262–7, 1992.

[15] A. Swillens, L. Lovstakken, J. Kips, H. Torp, and P. Segers, "Ultrasound simulation of complex flow velocity fields based on computational fluid dynamics", *IEEE Trans Ultrason Ferroelectr Freq Control*, vol. 56, no. 3, pp. 546–56, 2009.

[16] A. Rodriguez-Molares, O. M. H. Rindal, O. Bernard, *et al.*, "The Ultrasound toolbox", in *IEEE International Ultrasonics Symposium*, IEEE, pp. 1–4.

[17] H. Torp and K. Kristoffersen, "Velocity matched spectrum analysis: A new method for suppressing velocity ambiguity in pulsed-wave doppler", *Ultrasound Med Biol*, vol. 21, no. 7, pp. 937–44, 1995.